*sclerosis*

MDPI

*Article*

# In Silico Evaluation of Effect and Molecular Modeling of SNPs in Genes Related to Amyotrophic Lateral Sclerosis

**Gustavo Ronconi Roza [1], Caroline Christine Pincela da Costa [1], Nayane Soares de Lima [1], Angela Adamski da Silva Reis [1,2] and Rodrigo da Silva Santos [1,2,*]**

[1] Neurogenetics Research Center, Institute of Biological Sciences (ICB II), Federal University of Goiás (UFG), Goiânia 74690-900, Goiás, Brazil; gustavoronconi@egresso.ufg.br (G.R.R.); carolinechristine@discente.ufg.br (C.C.P.d.C.); nayanelima@discente.ufg.br (N.S.d.L.); angela@ufg.br (A.A.d.S.R.)

[2] Department of Biochemistry and Molecular Biology, Institute of Biological Sciences (ICB II), Federal University of Goiás (UFG), Goiânia 74690-900, Goiás, Brazil

* Correspondence: rdssantos@ufg.br

## Abstract

**Background**: Amyotrophic lateral sclerosis is a systemic, complex, multifactorial, and fatal neurodegenerative disease with various factors involved in its etiology. This study aimed to understand the effects of SNPs in the MTHFR, MTR, SLC19A1, and VAPB genes on protein functionality and structure and their influence on ALS susceptibility. **Methods**: The dbSNP and ClinVar databases were used for SNP data annotation, while UniProt and PDB provided protein sequences. We performed functional and structural predictions of SNPs using PolyPhen-2 and SNAP2. We modeled mutant proteins using AlphaFold 2 and visualized them in PyMOL to compare native and mutant forms. **Results**: Our results identified SNP rs74315431 as pathogenic, inducing structural and functional changes and exhibiting visible alterations in the three-dimensional structure. Although predicted as non-pathogenic, SNPs rs1801131, rs1805087, and rs1051266 caused protein structural alterations, a finding confirmed by three-dimensional visualization. SNP rs1801133 diverged from the others, being predicted as pathogenic but without causing changes in protein structure or function. **Conclusions**: Our study found a strong correlation between SNAP2-predicted alterations and those predicted by AlphaFold 2, whereas PolyPhen-2 results did not directly correlate with three-dimensional structure changes.

**Keywords:** neurodegeneration; Hyperhomocysteinemia; membrane contact sites; computational analysis; protein structural perturbation



Academic Editors: Maurizio A. Leone and Radu Tanasescu

Received: 21 June 2025
Revised: 28 July 2025
Accepted: 31 July 2025
Published: 5 August 2025

**Citation:** Roza, G.R.; da Costa, C.C.P.; de Lima, N.S.; da Silva Reis, A.A.; da Silva Santos, R. In Silico Evaluation of Effect and Molecular Modeling of SNPs in Genes Related to Amyotrophic Lateral Sclerosis. *Sclerosis* **2025**, *3*, 27. https://doi.org/10.3390/sclerosis3030027



## 1. Introduction

Amyotrophic lateral sclerosis (ALS) is a rare systemic and fatal neurodegenerative disease, with higher incidence after 60 years [1]. Roughly 2 out of every 100,000 individuals per year are affected worldwide [2]. Higher incidence rates have been reported in some European populations, such as those in Ireland and Scotland, reaching 2.6 cases per 100,000. In contrast, lower rates are observed in Eastern and Southern Asian populations, with 0.8 and 0.7 cases per 100,000, respectively [3]. In Brazil, despite limited studies and high levels of miscegenation, the estimated incidence ranges between 0.9 and 1.5 per 100,000 [4].

ALS presents different phenotypes according to age, sex, and genetic factors and is characterized by the degeneration of both upper and lower motor neurons leading to motor and non-motor symptoms [1,3]. It presents significant clinical variations, ranging

from muscle weakness in the limbs, dysarthria, and dysphagia to behavioral changes and cognitive decline [5].

The biogenesis of ALS is complex and multifactorial, involving several cellular and genetic mechanisms, and remains incompletely understood. However, both environmental factors, such as glutamatergic excitotoxicity, mitochondrial dysfunction, oxidative stress, protein aggregation, and neurotoxicity, and genetic factors are known to contribute to the disease's etiology [4,6]. These factors may act synergistically by triggering pathological mechanisms that lead to motor neuron cell death, although the specific contribution of each cannot be entirely quantified. Consequently, each case of ALS results from a combination of different mechanisms, not necessarily all simultaneously active [3].

Hyperhomocysteinemia (HHcy) is caused by the accumulation of homocysteine (Hcy), a sulfur-containing amino acid, which exerts a toxic effect through increased oxidative stress, resulting in inflammatory reactions, and the reduction of nitric oxide [7], promoting neurological damage and increasing susceptibility to ALS [8]. The folate pathway, or One-Carbon metabolism, is connected to the maintenance of normal levels of Hcy in the body by mediating the remethylation of Hcy into Methionine through the transfer of a methyl group [9]. Variants in genes involved in this pathway, such as *MTHFR* rs1801131 and rs1801133, *MTR* rs1805087, and *SLC19A1* rs1051266, produce, independently, dysfunctional proteins that negatively influence the homeostasis of Hcy, leading to the accumulation of this amino acid in the body [10].

Mitochondrial dysfunction is closely related to ALS. Alterations in mitochondrial functions, due to, among other reasons, impaired protein homeostasis, lead to the loss of function of homologous proteins, as is the case with the rs74315431 variant of the *VAPB* gene [11]. Among its functions, the VAPB protein constitutes bridges of contact between membranes (MCS), mainly between the endoplasmic reticulum (ER) and mitochondria (Mitochondria–Endoplasmic reticulum Contact Site, or MERCS), through which lipid and calcium ion transport occur (Ca2+) from ER from mitochondria. The loss of function of this protein disrupts the formation of MERCs and impacts calcium transport, consequently reducing the capacity for mitochondrial oxidative phosphorylation. Mitochondrial failure leads to mitophagic processes, disrupting cellular and neural ion homeostasis and potentially leading to cellular apoptosis and neurodegeneration [11,12].

Understanding the increase in oxidative stress as a point of convergence of the mentioned mechanisms and the consequent association with mitochondria, the main producer of reactive oxygen species (ROS), it is possible to postulate a hypothesis for ALS biogenesis. Thus, this study aimed to evaluate whether single-nucleotide polymorphisms (SNPs) in genes related to the folate pathway (*MTHFR*, *MTR*, and *SLC19A1*) and in the *VAPB* gene may alter the three-dimensional structure or stability of the encoded proteins, potentially contributing to the susceptibility or progression of amyotrophic lateral sclerosis (ALS).

## 2. Materials and Methods

This study followed best practices for in silico functional and structural analysis of SNPs using bioinformatics tools. Where applicable, our methodological description aligns with items from the STREGA (Strengthening the Reporting of Genetics Association Studies) guideline to ensure transparency, reproducibility, and clarity [13].

The selection of SNPs was based on their location in genes previously linked to homocysteine metabolism or cellular stress responses involved in ALS: *MTHFR*, *MTR*, *SLC19A1*, and *VAPB*. Information concerning the genes was obtained from the National Center for Biotechnology Information (NCBI) database [14]. We retrieved variant information from the dbSNP and ClinVar databases, prioritizing non-synonymous variants with existing clinical annotations and biological relevance.

This study was conducted exclusively with public, anonymized data, without direct involvement of humans or animals. Only computational data from public databases was utilized. Therefore, it did not require ethics committee approval. All analyses followed the ethical guidelines applicable to in silico studies.

We collected the FASTA sequences of the protein from the UniProt database [15]. The three-dimensional (3D) protein structures are available from the Protein Data Bank (PDB) [16]. It is important to highlight that the 3D structures of the MTHFR and SLC19A1 proteins on PDB are derived from experimental techniques for resolving protein structures, such as X-ray crystallography and cryo-electron microscopy, respectively. The 3D structures of MTR and VAPB proteins in the PDB do not include experimental data; only computational predictions of their conformations are available, generated by the AlphaFold 2 algorithm.

We copied the FASTA sequences of the proteins in their wild state from UniProt to a text file and then modified them manually by replacing the normal amino acid with the mutant amino acid at the position where the substitution occurs. The mutant amino acids are highlighted in the table below (Table 1).

Subtitle: In this table, we present a genetic panel of the *MTHFR*, *MTR*, *SLC19A1*, and *VAPB* genes, including detailed information on SNPs obtained from the dbSNP and ClinVar databases. In addition, we extracted the sequences of the respective proteins from the UniProt database. The table shows the FASTA sequences of the mutant proteins, highlighting the specific amino acid substitutions caused by the SNPs analyzed in our study.

The unaltered FASTA sequences of the proteins, collected from the UniProt database, served as input for the SNAP2 tool [17], a tool for identifying potential polymorphisms that predict the effect of the polymorphic variant on the molecular function of the protein. This tool generates a table with the potential polymorphisms at all amino acid positions in the protein, indicating the result of the substitution by the mutant, whether it is neutral or has an effect, the score of the result, and the accuracy of the prediction [18].

We analyzed the polymorphic protein sequences using the PolyPhen-2 tool, which predicts the potential impact of amino acid substitutions on protein structure and function [19]. The tool assigns a score from 0 to 1, estimating the likelihood of a substitution being damaging, with scores above 0.85 interpreted as probably damaging. PolyPhen-2 provides two predictive models: HumDiv and HumVar. PolyPhen-2 uses two different models: HumDiv and HumVar. The HumDiv model is trained on mutations that affect molecular function and cause Mendelian diseases. It also includes differences between human proteins and their mammalian homologs from UniProt. This model is best for evaluating rare variants that may be involved in complex traits. The HumVar model is trained on both disease-causing mutations and common non-synonymous SNPs (nsSNPs) that are not linked to diseases. These common variants are treated as benign. HumVar is more suitable for clinical diagnostics of monogenic diseases, where clear pathogenic effects are expected. Each model provides sensitivity and specificity scores. Sensitivity shows how well the model detects harmful variants. Specificity shows how well it identifies benign ones [20].

**Table 1.** Genetic panel of the four genes and their respective information obtained from the databases, along with the FASTA sequence of the mutant proteins with the alteration in the respective substituted amino acid.

| GENE | UniProt CODE | PDB CODE | SNP | Substitution | FASTA |
|---|---|---|---|---|---|
| *VAPB* | O95292 | AF_AFO95292F1 | rs74315431 | Pro56Ser (P56S) | MAKVEQVLSLEPQHELKFRGPFTDVVTTNLKLGNPTDRNV CFKVKTTAPRRYCVR**S**NSGIIDAGASINVSVMLQPFDYDPN EKSKHKFMVQSMFAPTDTSDMEAVWKEAKPEDLMDSKLRC VFELPAENDKPHDVEINKIISTTASKTETPIVSKSLSSSLDDTEV KKVMEECKRLQGEVQRLREENKQFKEEDGLRMRKTVQSNS PISALAPTGKEEGLSTRLLALVVLFFIVGVIIGKIAL |
| *MTHFR* | P42898 | 6FCX | rs1801133 | Ala222Val (A222V) | MVNEARGNSSLNPCLEGSASSGSESSKDSSRCSTPGLDPERHE RLREKMRRRLESGDKWFSLEFFPPRTAEGAVNLISRFDRMAA GGPLYIDVTWHPAGDPGSDKETSSMMIASTAVNYCGLETILH MTCCRQRLEEITGHLHKAKQLGLKNIMALRGDPIGDQWEE EEGGFNYAVDLVKHIRSEFGDYFDICVAGYPKGHPEAGSFEA DLKHLKEKVSAG**V**DFIITQLFFEADTFFRFVKACTDMGITCPI VPGIFPIQGYHSLRQLVKLSKLEVPQEIKDVIEPIKDNDAAIRN YGIELAVSLCQELLASGLVPGLHFYTLNREMATTEVLKRLGM WTEDPRRPLPWALSAHPKRREEDVRPIFWASRPKSYIYRTQE WDEFPNGRWGNSSSPAFGELKDYYLFYLKSKSPKEELLKMW GEELTSEESVFEVFVLYLSGEPNRNGHKVTCLPWNDEPLAAE TSLLKEELLRVNRQGILTINSQPNINGKPSSDPIVGWGPSGGY VFQKAYLEFFTSRETAEALLQVLKKYELRVNYHLVNVKGENI TNAPELQPNAVTWGIFPGREIIQPTVVDPVSFMFWKDEAFAL WIERWGKLYEEESPSRTIIQYIHDNYFLVNLVDNDFPLDNCLW QVVEDTLELLNRPTQNARETEAP |
| | | | rs1801131 | Glu429Ala (E429A) | MVNEARGNSSLNPCLEGSASSGSESSKDSSRCSTPGLDPERHE RLREKMRRRLESGDKWFSLEFFPPRTAEGAVNLISRFDRMAA GGPLYIDVTWHPAGDPGSDKETSSMMIASTAVNYCGLETILH MTCCRQRLEEITGHLHKAKQLGLKNIMALRGDPIGDQWEE EEGGFNYAVDLVKHIRSEFGDYFDICVAGYPKGHPEAGSFEA DLKHLKEKVSAGADFIITQLFFEADTFFRFVKACTDMGITCPI VPGIFPIQGYHSLRQLVKLSKLEVPQEIKDVIEPIKDNDAAIRN YGIELAVSLCQELLASGLVPGLHFYTLNREMATTEVLKRLGM WTEDPRRPLPWALSAHPKRREEDVRPIFWASRPKSYIYRTQE WDEFPNGRWGNSSSPAFGELKDYYLFYLKSKSPKEELLKMW GEELTSEESVFEVFVLYLSGEPNRNGHKVTCLPWNDEPLAAE TSLLKE**A**LLRVNRQGILTINSQPNINGKPSSDPIVGWGPSGGY VFQKAYLEFFTSRETAEALLQVLKKYELRVNYHLVNVKGENI TNAPELQPNAVTWGIFPGREIIQPTVVDPVSFMFWKDEAFAL WIERWGKLYEEESPSRTIIQYIHDNYFLVNLVDNDFPLDNCL WQVVEDTLELLNRPTQNARETEAP |

**Table 1.** *Cont.*

| GENE | UniProt CODE | PDB CODE | SNP | Substitution | FASTA |
|---|---|---|---|---|---|
| *MTR* | Q99707 | AF_AFQ99707F1 | rs1805087 | Aps919Gly (D919G) | MSPALQDLSQPEGLKKTLRDEINAILQKRIMVLDGGMGTMIQR<br>EKLNEEHFRGQEFKDHARPLKGNNDILSITQPDVIYQIHKEYLLAG<br>ADIIETNTFSSTSIAQADYGLEHLAYRMNMCSAGVARKAAEEVTLQ<br>TGIKRFVAGALGPTNKTLSVSPSVERPDYRNITFDELVEAYQEQAKGL<br>LDGGVDILLIETIFDTANAKAALFALQNLFEEKYAPRPIFISGTIVDKSG<br>RTLSGQTGEGFVISVSHGEPLCIGLNCALGAAEMRPFIEIIGKCTTAYV<br>LCYPNAGLPNTFGDYDETPSMMAKHLKDFAMDGLVNIVGGCCGST<br>PDHIREIAEAVKNCKPRVPPATAFEGHMLLSGLEPFRIGPYTNFVNIGE<br>RCNVAGSRKFAKLIMAGNYEEALCVAKVQVEMGAQVLDVNMDDG<br>MLDGPSAMTRFCNLIASEPDIAKVPLCIDSSNFAVIEAGLKCCQGKCI<br>VNSISLKEGEDDFLEKARKIKKYGAAMVVMAFDEEGQATETDTKIRV<br>CTRAYHLLVKKLGFNPNDIIFDPNILTIGTGMEEHNLYAINFIHATKVI<br>KETLPGARISGGLSNLSFSFRGMEAIREAMHGVFLYHAIKSGMDMGI<br>VNAGNLPVYDDIHKELLQLCEDLIWNKDPEATEKLLRYAQTQGTG<br>GKKVIQTDEWRNGPVEERLEYALVKGIEKHIIEDTEEARLNQKKYPR<br>PLNIIEGPLMNGMKIVGDLFGAGKMFLPQVIKSARVMKKAVGHLIPF<br>MEKEREETRVLNGTVEEEDPYQGTIVLATVKGDVHDIGKNIVGVVLG<br>CNNFRVIDLGVMTPCDKILKAALDHKADIIGLSGLITPSLDEMIFVAK<br>EMERLAIRIPLLIGGATTSKTHTAVKIAPRYSAPVIHVLDASKSVVVCS<br>QLLDENLKDEYFEEIMEEYEDIRQ**G**HYESLKERRYLPLSQARKSGFQ<br>MDWLSEPHPVKPTFIGTQVFEDYDLQKLVDYIDWKPFFDVWQLRGK<br>YPNRGFPKIFNDKTVGGEARKVYDDAHNMLNTLISQKKLRARGVV<br>GFWPAQSIQDDIHLYAEAAVPQAAEPIATFYGLRQQAEKDSASTEPY<br>YCLSDFIAPLHSGIRDYLGLFAVACFGVEELSKAYEDDGDDYSSIMVK<br>ALGDRLAEAFAEELHERVRRELWAYCGSEQLDVADLRRLRYKGIRPA<br>PGYPSQPDHTEKLTMWRLADIEQSTGIRLTESLAMAPASAVSGLYFSN<br>LKSKYFAVGKISKDQVEDYALRKNISVAEVEKWLGPILGYDTD |
| *SLC19A1* | P41440 | 7XTK | rs1051266 | His27Arg<br>(H27R) | MVPSSPAVEKQVPVEPGPDPELRSWR**R**LVCYLCFYGFMAQIRPGESFI<br>TPYLLGPDKNFTREQVTNEITPVLSYSYLAVLVPVFLLTDYLRYTPVLL<br>LQGLSFVSVWLLLLLGHSVAHMQLMELFYSVTMAARIAYSSYIFSLVR<br>PARYQRVAGYSRAAVLLGVFTSSVLGQLLVTVGRVSFSTLNYISLAFLT<br>FSVVLALFLKRPKRSLFFNRDDRGRCETSASELERMNPGPGGKLGHA<br>LRVACGDSVLARMLRELGDSLRRPQLRLWSLWWVFNSAGYYLVVYY<br>VHILWNEVDPTTNSARVYNGAADAASTLLGAITSFAAGFVKIRWAR<br>WSKLLIAGVTATQAGLVFLLAHTRHPSSIWLCYAAFVLFRGSYQFLVP<br>IATFQIASSLSKELCALVFGVNTFFATIVKTIITFIVSDVRGLGLPVRKQF<br>QLYSVYFLILSIIYFLGAMLDGLRHCQRGHHPRQPPAQGLRSAAEEK<br>AAQALSVQDKGLGGLQPAQSPPLSPEDSLGAVGPASLEQRQSDPYLA<br>QAPAPQAAEFLSPVTTPSPCTLCSAQASGPEAADETCPQLAVHPPGV<br>SKLGLQCLPSDGVQNVNQ |

Labeled amino acids refer to the sequence of the mutant proteins with the alteration in the respective substituted amino acid.

Structural modeling of the mutant proteins was performed using Colab Fold (version 1.5.2). This algorithm, available in the Google Colab virtual environment, predicts the tertiary structures of proteins through alignment calculations that compare the overlap of amino acid sequences with protein sequences present in the PDB [21–23]. To increase the reliability of the result, various other parameters are utilized, such as calculating the degree of interaction forces between amino acids and between protein chains, making AlphaFold 2 the gold standard among protein modeling and prediction methods [23]. AlphaFold 2 generates, as a prediction result, 5 likely models of protein conformation, ranked from 1 (highest accuracy) to 5 (lowest accuracy), predicted local distance difference (pLDDT) plot, and predicted aligned error (PAE) plot, representing predicted aligned errors between residue pairs.

We visualized the predicted proteins using PyMOL (version 2.0.7) software [19], a viewer for three-dimensional molecular structure. PyMOL has access to the PDB databases and allows the importation of proteins for visualization using the PDB code of the protein of interest [24]. Proteins colored in cyan originate from the PDB database, whereas those in green result from ColabFold predictions. We generated all images of the wild-type and polymorphic proteins using the image export tool in PyMOL.

## 3. Results

### *3.1. Analysis of SNP Effect*

For the VAPB protein, both SNAP2 and PolyPhen-2 showed a damaging effect of the polymorphism rs74315431 on protein function and structure. SNAP2 gave a high damaging score of 97 (accuracy: 95%). PolyPhen-2 scored 1 in both HumDiv and HumVar models. The sensitivity (0.00) and specificity (1.00) values mean that PolyPhen-2 did not detect any true damaging variants in this case but correctly identified benign variants.

For the MTHFR protein, the rs1801133 SNP was predicted by SNAP2 to have a neutral effect, with a score of −47 (accuracy: 72%). In PolyPhen-2, HumDiv classified this SNP as damaging (score 0.996), while HumVar labeled it possibly damaging (score 0.712). Sensitivity and specificity values indicate how well the models detect damaging variants (sensitivity) and correctly identify benign ones (specificity). For example, HumDiv has moderate sensitivity (0.55) and high specificity (0.98), meaning it detects about half of damaging variants and rarely misclassifies benign variants. The rs1801131 SNP in MTHFR showed a slight effect in SNAP2 (score 6, accuracy 53%). PolyPhen-2 classified this mutation as benign with low scores (0.021 for HumDiv and 0.009 for HumVar). The sensitivity and specificity values suggest that the models are good at recognizing benign variants (specificity around 0.80–0.96) but differ in sensitivity.

For the MTR protein variant rs1805087, SNAP2 indicated structural and functional effects (score 3, accuracy 53%). However, PolyPhen-2 classified it as benign in both models, with scores around 0.16. Sensitivity and specificity values show that the models correctly identify most benign variants and have good accuracy in this context.

Finally, the SLC19A1 protein variant rs1051266 was predicted by SNAP2 to have an effect (score 2, accuracy 53%). PolyPhen-2 classified this SNP as benign with a score of 0 in both HumDiv and HumVar. A sensitivity of 1.00 indicates that the models detect all damaging variants, but a specificity of 0.00 means that they misclassify benign variants in this case.

### *3.2. Variant Structure Prediction*

The Colab Fold generated graphs indicating the quality of the predicted structure based on database references and algorithm calculations. The predicted local distance difference test (pLDDT) is a per-residue measure of local confidence, ranging from 0 to 100,

with 100 indicating maximum confidence. Below 50, the confidence is very low; between 50 and 70, it is low; between 70 and 90, it is high; and between 90 and 100, it is very high. When there is limited data available in databases, the predicted location is considered of low confidence. Predicted aligned error (PAE) measures the relative error in the location between two residues within a predicted structure. Lower PAE values indicate higher confidence in the relative position of residues in the predicted structure, while higher values indicate lower confidence. The PAE plot is a heatmap where deep blue indicates a value of 0 and deep red indicates a value of 1.

#### 3.2.1. VAPB p.P56S

For the VAPB S56 protein, at position 56, the confidence measure of the local structure of the residue is above 90 (Figure 1). The intense blue block that covers residues 1–125 highlights the confidence of the relative position of these residues and adequate packaging of the protein in this region, visually evidenced (Figure 2). It is possible to observe changes in the three-dimensional structure between the native protein and the mutant protein, noting the gain of a carboxyl group in VAPB p.P56S, indicated by the red color (Figure 3b), compared to native VAPB (Figure 3a), caused by the substitution of a proline for a serine.

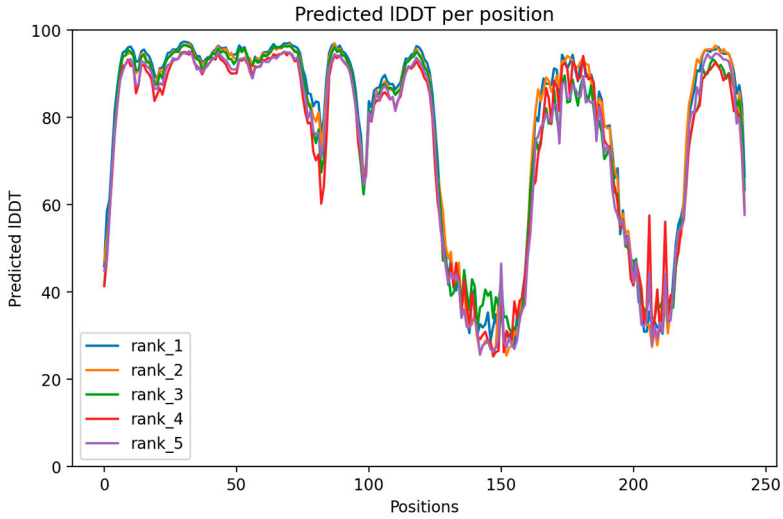


**Figure 1.** pLDDT plot indicates the reliability from 0 to 100 of the local relative position of each amino acid in the five generated models for the VAPB p.P56S predicted protein structure. Different colors indicate protein conformations, ranked from 1 (highest accuracy) to 5 (lowest accuracy).

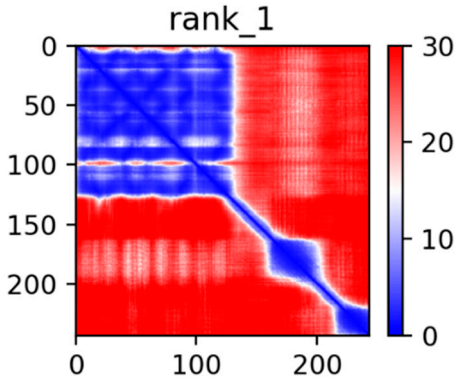


**Figure 2.** PAE plot of the best out of five models, showing regions of high confidence (blue) and low confidence (red) for the predicted structure of VAPB p.P56S.

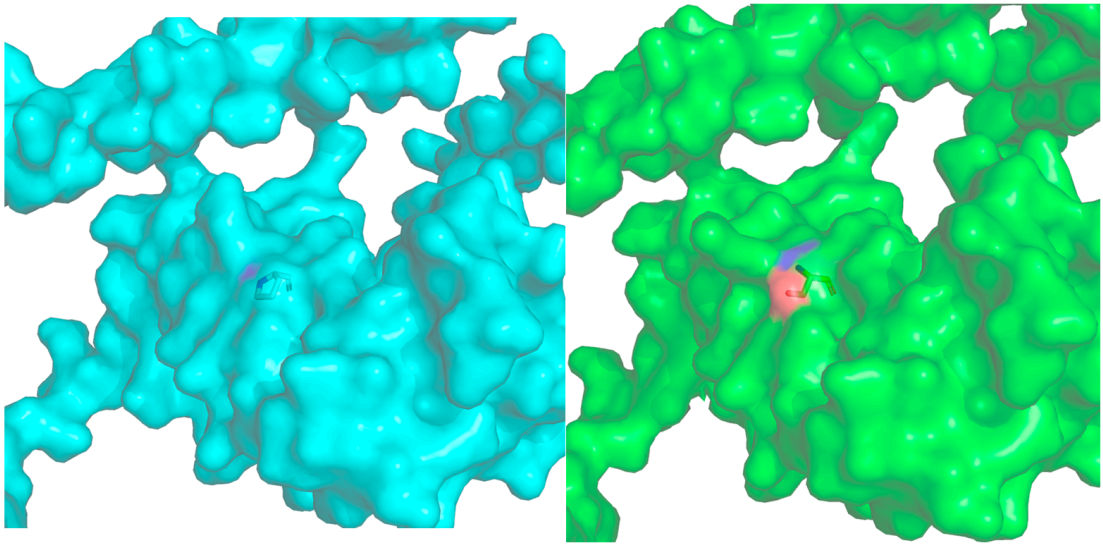

(**a**) (**b**)

**Figure 3.** Comparative panel of the structure of the native VAPB protein and the mutant VAPB, predicted in the Colab Fold and visualized in the PyMol, with a focus on amino acids. (**a**) Proline at position 56 of the native protein (cyan). (**b**) Serine at position 56 of the mutant protein (green).

#### 3.2.2. MTHFR Variants (p.A222V and p.E429A)

For the residue change at position 222, the local confidence measure of the residue is above 90 (Figure 4). The high confidence in proper packing and the relative positioning of residues 48–337 is visually evidenced by the intense blue block (Figure 5). The maintenance of only one carboxyl group, indicated by the red color, and the three-dimensional structures of the MTHFR p.A222V form (Figure 6b) and native MTHFR (Figure 6a) are observed, without visually significant changes caused by the substitution of an alanine for a valine.

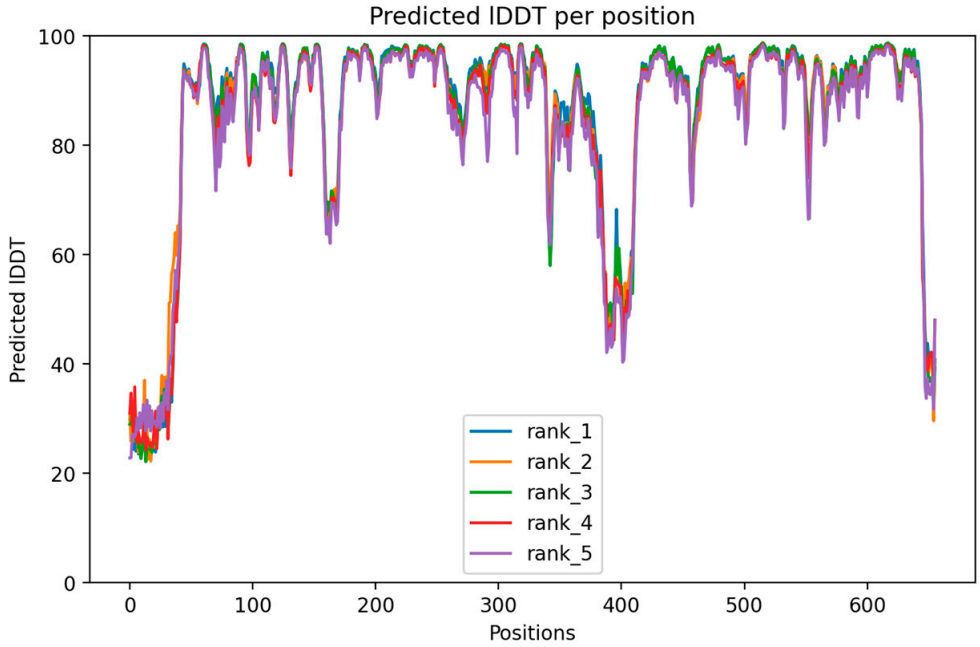


**Figure 4.** pLDDT plot indicates the reliability from 0 to 100 of the local relative position of each amino acid in the five generated models for the MTHFR p.A222V predicted protein structure. Different colors indicate protein conformations, ranked from 1 (highest accuracy) to 5 (lowest accuracy).

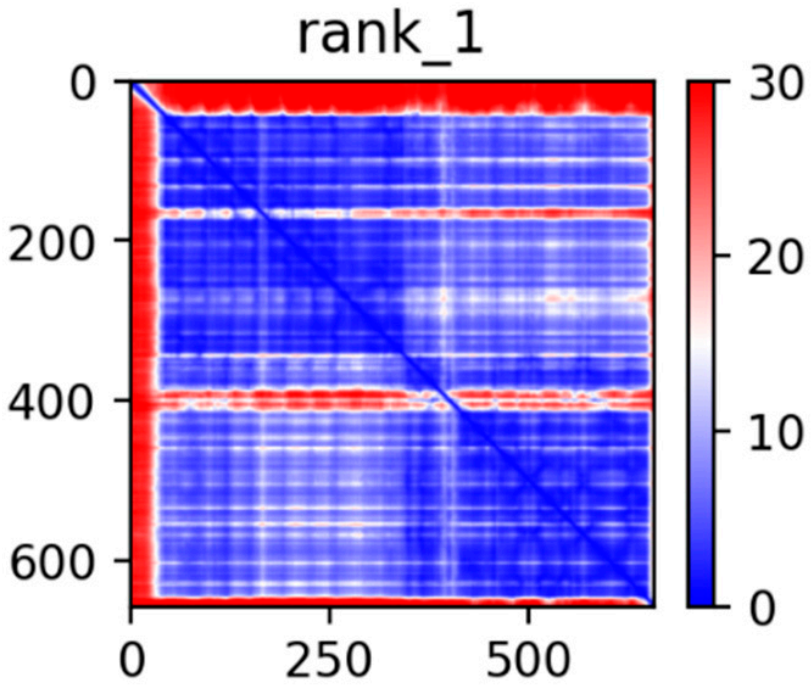


**Figure 5.** PAE plot of the best out of five models, showing regions of high confidence (blue) and low confidence (red) for the predicted structure of MTHFR p.A222V.

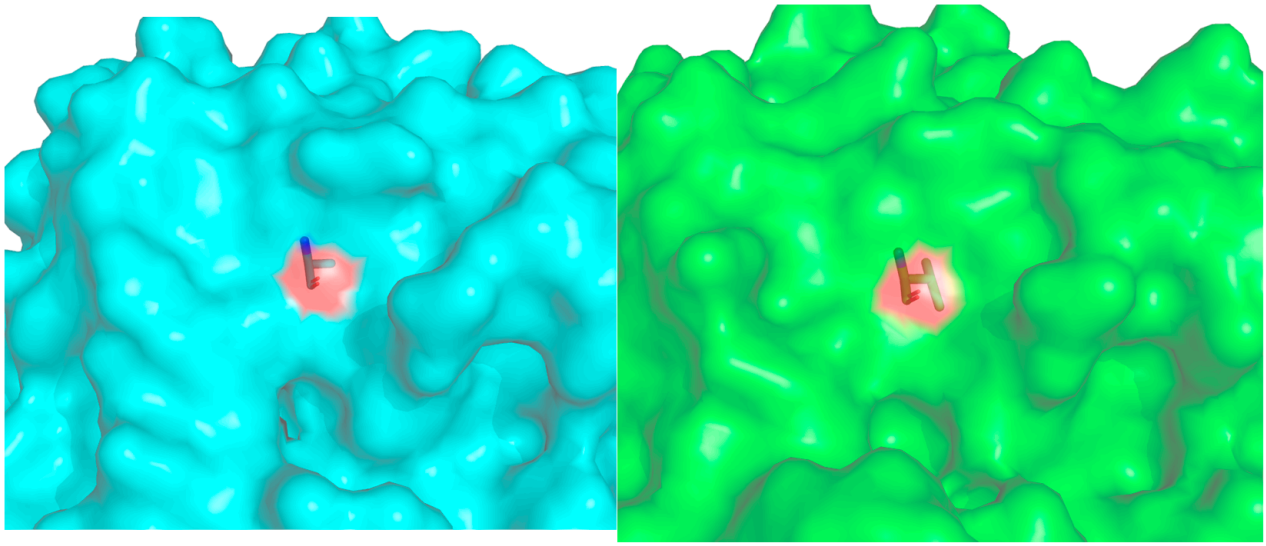

(**a**) (**b**)

**Figure 6.** Comparative panel of the structure of the native MTHFR protein and the mutant MTHFR, predicted in the Colab Fold and visualized in the PyMol, with a focus on amino acids. (**a**) Alanine at position 222 of the native protein (cyan). (**b**) Valine at position 222 of the mutant protein (green).

For the residue change at position 429, the local residue prediction measure is close to 90 (Figure 7). The high confidence in proper packing and the relative positioning of residues 363–644 is marked by the strong blue coloration (Figure 8). It is possible to observe the loss of two carboxyl groups, indicated by the red color, and the addition of an amino group, indicated by the blue color, in the MTHFR p.E429A protein (Figure 9b) compared to the native form (Figure 9a) and the possible structural changes caused by the substitution of glutamine for an alanine.

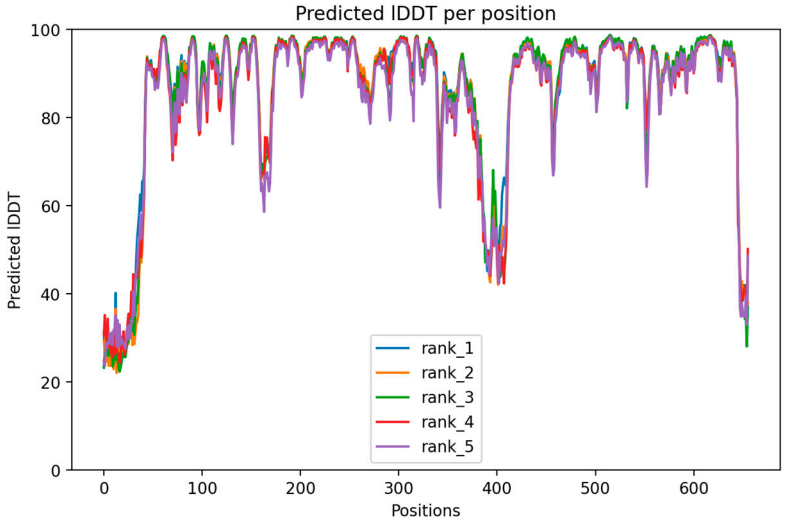


**Figure 7.** pLDDT plot indicates the reliability from 0 to 100 of the local relative position of each amino acid in the five generated models for the MTHFR p.E429A predicted protein structure. Different colors indicate protein conformations, ranked from 1 (highest accuracy) to 5 (lowest accuracy).

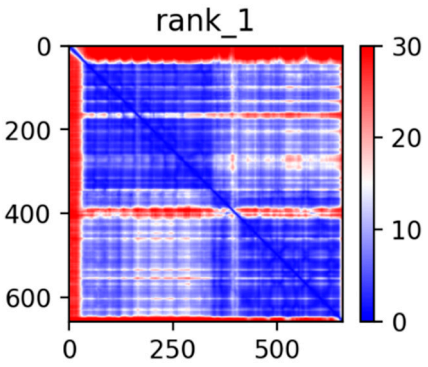


**Figure 8.** PAE plot of the best out of five models, showing regions of high confidence (blue) and low confidence (red) for the predicted structure of MTHFR p.E429A.

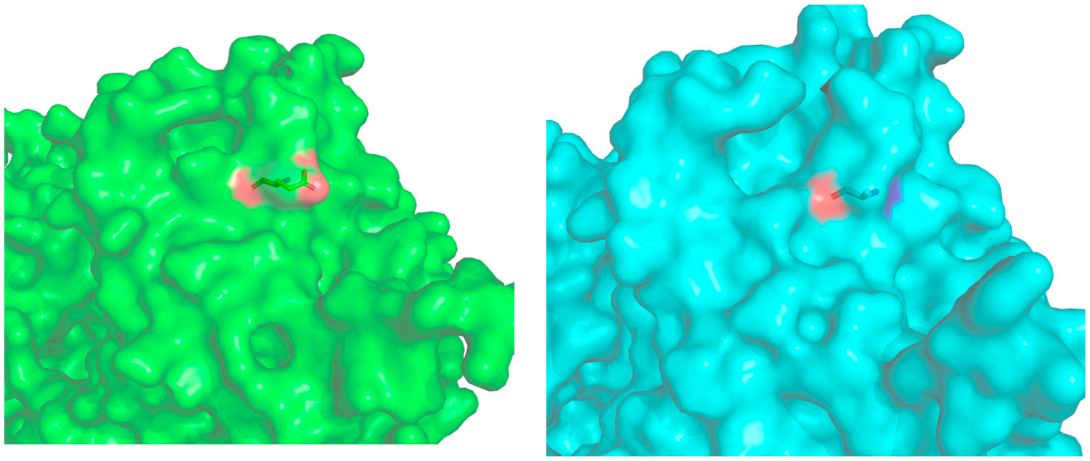

(**a**) (**b**)

**Figure 9.** Comparative panel of the structure of the native MTHFR protein and the mutant MTHFR, predicted in the Colab Fold and visualized in the PyMol, with a focus on amino acids. (**a**) Glutamine at position 429 of the native protein (cyan). (**b**) Alanine at position 429 of the mutant protein (green).

### 3.2.3. MTR p.D919G

The plot generated for the MTR protein overall shows significant variations in the local residue prediction measure. Therefore, for position 919, it ranges between values

of 70–90 (Figure 10). In Figure 11, two delimited regions can be observed, 11–651 and 662–1265, both with clear regions present, but more prominent in the second region where position 919 is located. These clear regions, with less defined boundaries, demonstrate reduced confidence in Colab Fold in predicting the exact position of the residues. The loss of two carboxyl groups, indicated by the red color, and the maintenance of the amino group, indicated by the blue color, is observed in MTR p.D919G (Figure 12b), compared to native MTR (Figure 12a), as well as possible structural changes resulting from the substitution of an aspartate for a glycine.

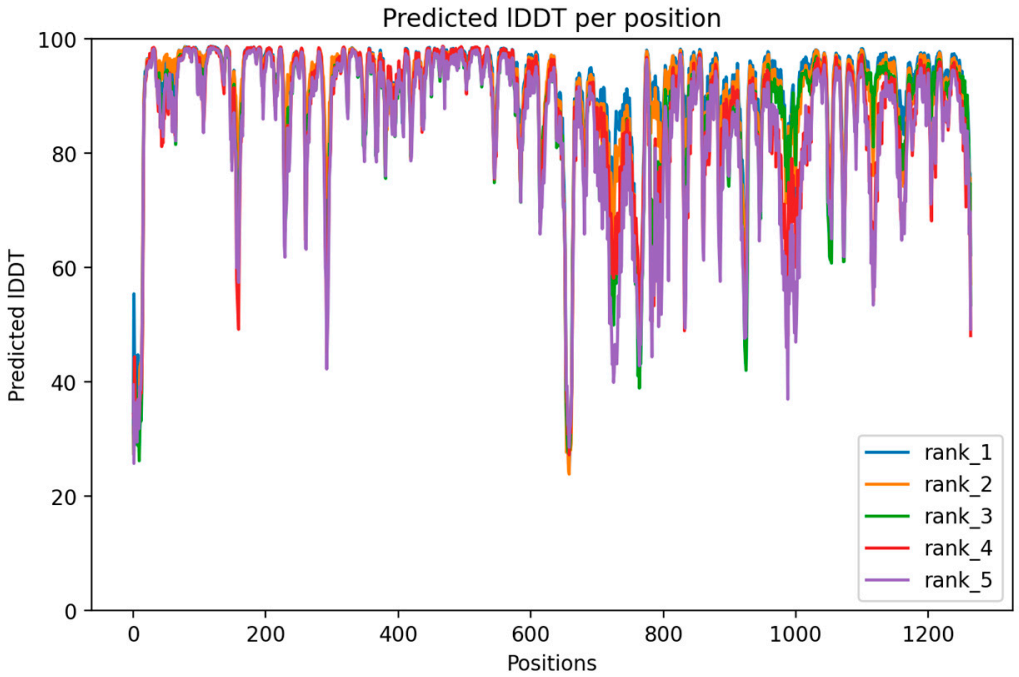


**Figure 10.** pLDDT plot indicates the reliability from 0 to 100 of the local relative position of each amino acid in the five generated models for the MTR p.D919G predicted protein structure. Different colors indicate protein conformations, ranked from 1 (highest accuracy) to 5 (lowest accuracy).

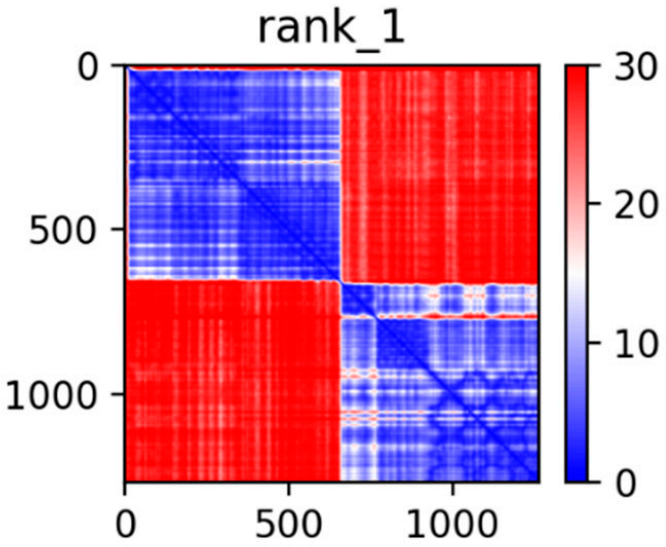


**Figure 11.** PAE plot of the best out of five models, showing regions of high confidence (blue) and low confidence (red) for the predicted structure of MTR p.D919G.

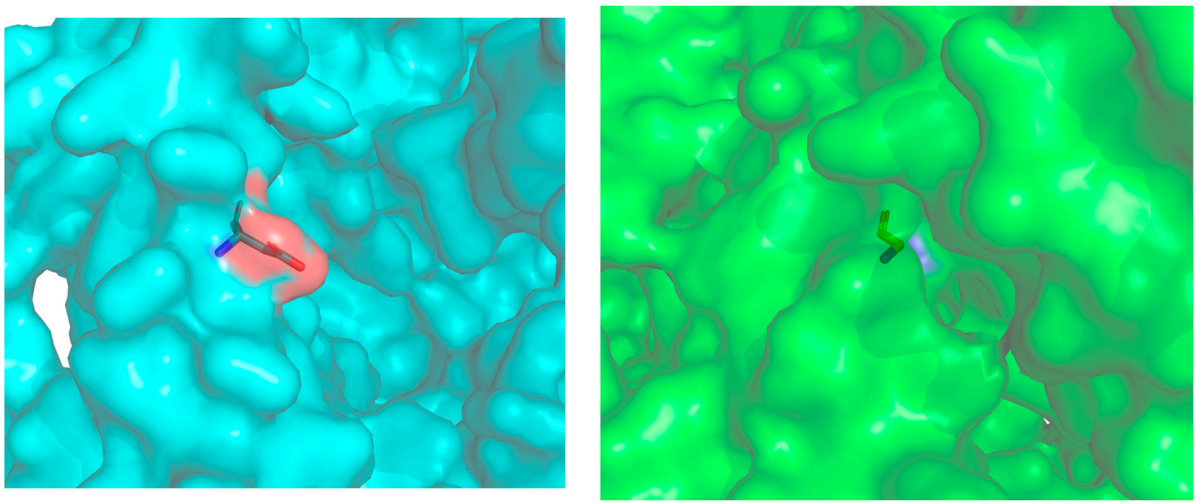

(**a**) (**b**)

**Figure 12.** Comparative panel of the structure of the native MTR protein and the mutant MTR, predicted in the Colab Fold and visualized in the PyMol, with a focus on amino acids. (**a**) Aspartate at position 919 of the native protein (cyan). (**b**) Glycine at position 919 of the mutant protein (green).

### 3.2.4. SLC19A1 p.H27R

The local prediction measure for the SLC19A1 p.H27R variant was around 60 (Figure 13). In Figure 14, well-defined residue groups can be identified, 18–205 and 245–461, with high confidence in proper packing and clearly marked relative positioning of residues indicated by intense blue coloration. It is possible to observe the gain of an amino, indicated by the blue color, and carboxyl group, indicated by the red color, in SLC19A1 p.H27R (Figure 15b) compared to SLC19A1 (Figure 15a) and the possible structural changes caused by the substitution of a histidine for an arginine.

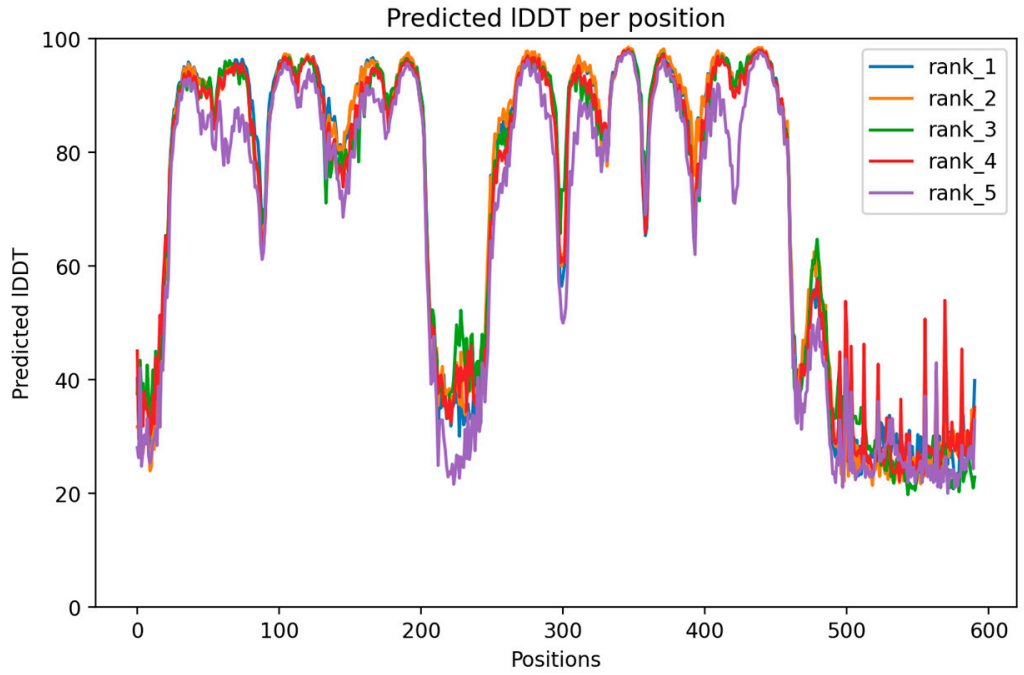


**Figure 13.** pLDDT plot indicating the reliability from 0 to 100 of the local relative position of each amino acid in the five generated models for the SLC19A1 p.H27R predicted protein structure. Different colors indicate protein conformations, ranked from 1 (highest accuracy) to 5 (lowest accuracy).

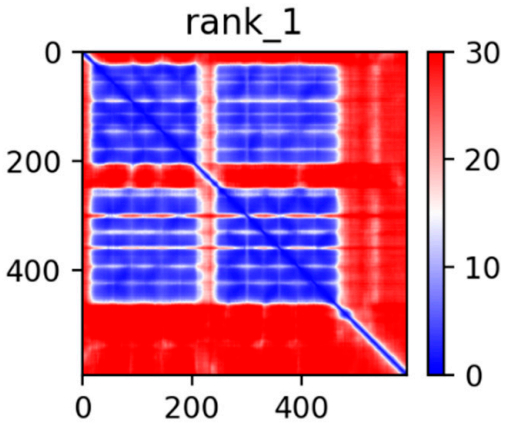


**Figure 14.** PAE plot of the best out of five models, showing regions of high confidence (blue) and low confidence (red) for the predicted structure of SLC19A1 p.H27R.

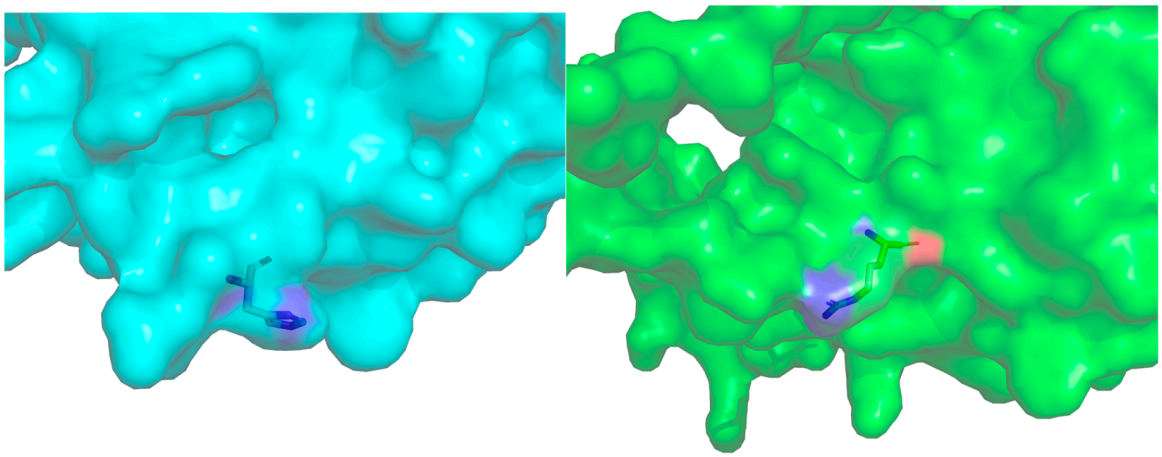

**(a)** **(b)**

**Figure 15.** Comparative panel of the structure of the native SLC19A1 protein and the mutant SLC19A1, predicted in the Colab Fold, and visualized in the PyMol, with a focus on amino acids. (**a**) Histidine at position 919 of the native protein (cyan). (**b**) Arginine at position 919 of the mutant protein (green).

## 4. Discussion

In this study, the heatmaps and scoring scales provided a visual and quantitative overview of the predicted effects of each SNP on protein structure and function. For example, the heatmap generated from SNAP2 scores highlighted the damaging impact of the *VAPB* p.P56S mutation, which corresponded with high damaging scores (above 90) and was corroborated by PolyPhen-2 predictions. Conversely, mutations such as *MTHFR* p.A222V showed neutral or benign scores on both platforms, which were visually reflected in the heatmaps by lower intensity signals. These graphical representations helped identify variants with potential clinical relevance by simplifying complex datasets into interpretable patterns, allowing us to prioritize mutations for further experimental validation and clinical consideration. Therefore, the heatmaps were not only descriptive tools but also crucial for interpreting the functional consequences of genetic variants in the context of neurodegenerative disease research.

Among the cases analyzed, it was noted that the VAPB p.P56S mutation stood out not only for its high scores in predictive tools but also for the structural changes observed at the

three-dimensional level, which reinforce its functional relevance. It is observed that both SNAP 2 and PolyPhen-2 indicated a detrimental effect of the mutations on the structure and functionality of the protein. In addition, the pLDDT and PAE plots demonstrate good reliability of the predicted mutant protein structure by Colab Fold in the region corresponding to the MSP domain, which is responsible for the protein's functions.

Currently, the VAPB protein lacks a 3D model derived from empirical data, so a predicted native structure generated by AlphaFold 2, available in the PDB database, was used. Comparisons of this predicted structure with the one available in the PDB reveal that the VAPB p.P56S variant shows some structural alterations compared to the native form (Figure 3), likely due to the substitution of proline, an aliphatic and nonpolar amino acid, with serine, a polar uncharged amino acid. This substitution introduces a carboxyl group into the protein structure, which can alter the forces of interactions among molecules around the substitution site. This aligns with previous findings indicating that the P56S mutation leads to remarkable changes in the biochemical and biological properties of the VABP protein [25].

Position 56, along with the entire MSP domain, was predicted with high confidence, as indicated by the pLDDT (Figure 1) and PAE (Figure 2) plots. The SNP C166T (rs74315431) causes a cytosine-to-thymine substitution at position 166 of the gene, resulting in the substitution of proline with serine at position 56 of the protein sequence. This amino acid substitution occurs at a conserved position in the MSP domain, adjacent to the FFAT binding site (two phenylalanines and an acidic tract), which leads to changes in the protein's structural dynamics and impairs the formation of MCSs and MERCS [12]. Furthermore, Kumar et al. reported that the SIFT algorithm identified rs74315431 as highly deleterious, and I-Mutant 3.0 predicted a decrease in protein stability for P56S. They suggest that these findings are crucial as nsSNPs can significantly alter the function of corresponding proteins by disrupting their structures [26]. This is consistent with the results obtained from SNAP 2 and PolyPhen 2, demonstrating that the proline-to-serine substitution indeed causes disturbances in the structure and functionality of the mutant protein.

*VAPB* is a prominent gene in the investigation of ALS in the Brazilian population. Its association with ALS was first discovered in Brazil [25], and it has since been identified as the gene most significantly related to the development of ALS, particularly in the Southeast region, which is the primary center for ALS studies in the country [27].

For SNP rs1801133, SNAP2 data reported the mutation has a neutral effect on the protein's functional structure, while PolyPhen-2 characterized the mutation as damaging to health. pLDDT (Figure 4) and PAE (Figure 5) plots generated by Colab Fold indicate high confidence in the predicted three-dimensional structure. In modeling performed by AlphaFold 2, MTHFR p.A222V showed no significant structural changes in its external structure (Figure 6), consistent with SNAP2's suggestion.

SNP C677T (rs1801133) is a non-synonymous point mutation, substituting cytosine with thymine at position 677 of the *MTHFR* gene, causing the substitution of alanine with valine at position 222 in the resulting protein's catalytic domain [28]. This mutation may act as a potential factor in the development of neuronal diseases [29,30]. Supporting PolyPhen-2 analysis, it has been observed that the substitution of alanine with valine (Figure 6), two nonpolar amino acids, reduces protein stability by increasing conformational flexibility and significantly decreasing the ability to form hydrogen bonds with the FAD ligand, a redox cofactor crucial for major metabolic reactions [31–33].

For MTHFR p.E429A, SNAP2 revealed that the mutation affects the protein's functional structure, while PolyPhen-2 considered the mutation benign for health, consistent with many studies that do not associate this SNP with different types of diseases [34–37]. Similarly to the previous case, pLDDT (Figure 7) and PAE (Figure 8) plots demonstrate high

reliability of the predicted tertiary structure. SNP A1298C (rs1801131) is a non-synonymous point mutation at position 1298, causing the substitution of adenine with cytosine, resulting in the substitution of glutamate with alanine at position 429 in the protein's regulatory domain, reducing protein thermal stability and enzymatic function [38] (p. 84), [39]. The mutant protein MTHFR p.E429A showed minor structural changes due to the substitution of negatively charged polar glutamate with nonpolar aliphatic alanine, reducing carboxyl groups and adding an amino group (Figure 9), supporting SNAP2's analyses. However, PolyPhen-2 suggested that the substitution does not cause any structural, functional, or disease-causing effects.

Both MTHFR p.E429A and MTHFR p.A222V mutations also showed a reduction in the number of hydrogen bonds when interacting with the FAD cofactor, albeit to a lesser extent [32]. Desai and Chauhan [33] also identified, through analysis of various *MTHFR* gene polymorphisms, that rs1801133 (A222V) and rs1801131 (E429A) have higher population allele frequencies but are not the most deleterious, whereas the most deleterious ones (R157Q, L323P, and W500C) are less frequent.

SNAP 2 data indicated that the p.D919G mutation affects the protein's functional structure, while PolyPhen-2 showed that the mutation has a benign effect on individual health. For this protein, the pLDDT plot (Figure 10) demonstrated significant variability in the local confidence measure of residues, while the PAE plot (Figure 11) revealed two regions of high confidence in relative positioning, but with noticeable areas of low confidence within these regions, indicating uncertainty in the algorithm's ability to predict the exact positions of residues. Currently, the MTR protein lacks an experimentally derived three-dimensional model in the PDB, reflecting a lack of experimental information about this protein, likely contributing to lower confidence in molecular structure prediction, including position 919, where the mutation occurred.

The commonly studied *MTR* polymorphism, SNP rs1805087 (A2756G), is a non-synonymous point mutation caused by the substitution of adenine with guanine at position 2756 of the gene, resulting in the substitution of aspartic acid with glycine at position 919 of the encoded enzyme, which can reduce enzymatic function and affect various cellular functions [35]. In the MTR G919 protein, the substitution of negatively charged polar aspartic acid with nonpolar aliphatic glycine showed visible alterations in the three-dimensional structure (Figure 12), including a reduction in the number of oxygen atoms and carboxyl groups, leaving only an amino group. Despite limited information, this mutation has been identified as an SNP of minor significance from a human health perspective, predicted to be neutral regarding disease development and a site of proteolytic cleavage [40].

Similarly to other mutations, except for MTHFR p.A222V, SNAP2 demonstrated that SLC19A1 p.H27R mutation affects the structure of the SLC19A1 R27 protein, while PolyPhen-2 predicted the mutation as benign. The pLDDT plot (Figure 13) for residue position 27 showed low local confidence (between 50 and 70), whereas the PAE plot (Figure 14) demonstrated confidence in the relative positioning of residues between 18 and 205 and between 245 and 461.

The gene *SLC19A1* encodes the protein known as SLC19A1, the primary folate carrier in the body, transporting preferentially reduced folates like methyl-THF and formyl-THF across the cell membrane. The A80G polymorphism (rs1051266) of the *SLC19A1* gene is a non-synonymous point mutation, substituting adenine with guanine at nucleotide position 80 of the gene, resulting in the substitution of histidine with arginine at position 27 of the intramembrane protein. This SNP alters protein function and may modulate the effects of *MTHFR* C677T, contributing to HHcy [38] (pp. 93–94).

Comparing the model of native SLC19A1 protein with predicted SLC19A1 R27, we observed that the substitution of histidine with arginine, both positively charged polar amino acids, resulted in a reduction of oxygen atoms but did not significantly alter the local structure of the region (Figure 15). Although the SNAP2 results indicate that the mutation affects the protein's structure and functionality, PolyPhen-2 indicates no detrimental effect of the mutation on human health. The mutation is located in the N-terminal loop, linking the S1 transmembrane domain, affecting the topology of half of all twelve domains, S1, S2, S4, S8, S9, and S10. It negatively impacts binding sites between the S8 and S9 and between the S9 and S10 domains, reducing folate affinity with the mutant protein [41], and supporting PolyPhen-2 analyses.

Predicting the functional effects of mutations and polymorphisms in genes and proteins through in silico tools has proven invaluable in studies associated with the pathogenesis of neurodegenerative diseases. The increasing availability of biological data and computational tools makes bioinformatics more accessible, facilitating data access and enabling robust analyses using public online databases and software such as NCBI, UniProt, Protein Data Bank, SNAP2, and PolyPhen-2, all utilized in this study. The virtual environment of AlphaFold 2, specifically Colab Fold, exemplifies this accessibility.

AlphaFold 2 can deliver various methodologies with complete libraries of single-domain protein structures, determine the relationship between amino acid sequences and their folds, and conduct diverse tests while applying quality controls to select the most reliable generated structures [42]. Beyond protein structure prediction, it is known that from scores calculated in pLDDT and PAE by AlphaFold 2, a more integrated view of protein interactions and movements of predicted proteins can be obtained [43]. Guo et al. [43] also state that low pLDDT scores may indicate regions of high residue flexibility, enhancing our understanding of protein function and allowing for reinterpretation of data presented in this study for areas with low pLDDT confidence.

The integration of in silico analyses, such as those performed with SNAP2, PolyPhen-2, and AlphaFold 2, offers valuable insights for clinical practice. By predicting the structural and functional impact of specific SNPs and mutations, clinicians can better interpret genetic test results, particularly in complex diseases like ALS and other neurodegenerative disorders. This information aids in distinguishing between benign variants and those likely to contribute to disease pathology, thus improving diagnostic accuracy. Furthermore, understanding the molecular consequences of mutations enables the identification of potential therapeutic targets and guides personalized treatment strategies. As precision medicine advances, such computational tools are becoming essential for timely and cost-effective genetic screening, risk assessment, and the development of targeted interventions, ultimately enhancing patient management and outcomes.

## 5. Limitations

This study has inherent limitations associated with in silico analyses. The main limitation is that the predictions of the structural and functional impacts of the analyzed SNPs were based on computational tools, such as SNAP2, PolyPhen-2, and AlphaFold 2, which, although robust, cannot replace experimental validation. Considering the interpretative difficulties of the results, which are based only on predictive algorithm evaluations, caution is needed when interpreting the results generated.

Another important point to consider is that the absence of experimentally determined 3D structures for some proteins may reduce the accuracy of structural modeling. In addition, the study did not incorporate molecular dynamics simulations, which could have provided deeper insights into the conformational flexibility and interaction of dynamics of mutant proteins.

Lastly, the study focused on a limited number of SNPs and genes. Even though these SNPs were selected based on their known biological relevance to the disease under investigation, other variants and molecular pathways may also contribute to ALS susceptibility and progression. Future studies integrating experimental validation, broader variant screening, and complementary in silico approaches should be considered to refine, confirm, and expand these findings.

## 6. Conclusions

This study assessed the effects caused by polymorphisms on the function and structure of mutant proteins, analyzing detrimental changes caused by these polymorphisms in the 3D structure compared to native forms. The study found a strong correlation between SNAP2-predicted alterations and those predicted by AlphaFold 2, while PolyPhen-2 results did not show a direct association with 3D structure. For nearly all proteins, except for the mutant MTR p.D919G, predicted alterations correlated with reduced protein efficiency.

For future analyses, approaches focusing on integrated molecular dynamics of proteins can provide deeper insights into how interactions between these mutations impair functionality, potentially advancing our understanding of their influence on susceptibility to developing ALS.

**Author Contributions:** Conceptualization, A.A.d.S.R. and R.d.S.S.; Methodology, G.R.R., C.C.P.d.C., N.S.d.L., A.A.d.S.R. and R.d.S.S.; Software, G.R.R., C.C.P.d.C. and N.S.d.L.; Validation, G.R.R., C.C.P.d.C., N.S.d.L., A.A.d.S.R. and R.d.S.S.; Formal Analysis, G.R.R., C.C.P.d.C. and N.S.d.L.; Investigation, G.R.R., C.C.P.d.C. and N.S.d.L.; Resources, A.A.d.S.R. and R.d.S.S.; Data Curation, G.R.R., C.C.P.d.C. and N.S.d.L.; Writing—Original Draft Preparation, G.R.R., C.C.P.d.C. and N.S.d.L.; Writing—Review and Editing, A.A.d.S.R. and R.d.S.S.; Supervision, A.A.d.S.R. and R.d.S.S.; Project Administration, A.A.d.S.R. and R.d.S.S.; Funding Acquisition, A.A.d.S.R. and R.d.S.S. All authors have read and agreed to the published version of the manuscript.

**Funding:** This research received no external funding.

**Institutional Review Board Statement:** Not applicable.

**Informed Consent Statement:** Not applicable.

**Data Availability Statement:** Data are contained within the article.

**Acknowledgments:** We thank the journal **Sclerosis** for the opportunity to contribute to this Special Issue, "Exploring Environmental Risk Factors for Disease Progression in Multiple Sclerosis and Amyotrophic Lateral Sclerosis".

**Conflicts of Interest:** The authors declare no conflicts of interest.

## References

1. Feldman, E.L.; Goutman, S.A.; Petri, S.; Mazzini, L.; Savelieff, M.G.; Shaw, P.J.; Sobue, G. Amyotrophic lateral sclerosis. *Lancet* **2022**, *400*, 1363–1380. [CrossRef]
2. Akçimen, F.; Lopez, E.R.; Landers, J.E.; Nath, A.; Chiò, A.; Chia, R.; Traynor, B.J. Amyotrophic lateral sclerosis: Translating genetic discoveries into therapies. *Nat. Rev. Genet.* **2023**, *24*, 642–658. [CrossRef]
3. Hardiman, O.; Al-Chalabi, A.; Chio, A.; Corr, E.M.; Logroscino, G.; Robberecht, W.; Shaw, P.J.; Simmons, Z.; Van Den Berg, L.H. Amyotrophic lateral sclerosis. *Nat. Rev. Dis. Primers* **2017**, *3*, 17071. [CrossRef]
4. Pereira, J.C.; Costa, J.O.; Costa, C.C.P.; Lima, N.S.; Barros, J.B.S.; Bento, D.C.P.; Reis, A.A.; Santos, R.S. Research Article New insights of miRNAs dysregulation in the molecular pathological basis of neurodegenerative sclerosis: A systematic review. *Genet. Mol. Res.* **2021**, *20*, gmr18843. [CrossRef]
5. Goutman, S.A.; Hardiman, O.; Al-Chalabi, A.; Chió, A.; Savelieff, M.G.; Kiernan, M.C.; Feldman, E.L. Recent advances in the diagnosis and prognosis of amyotrophic lateral sclerosis. *Lancet Neurol.* **2022**, *21*, 480–493. [CrossRef]

6. de Lima, N.S.; da Costa, C.C.P.; Assunção, L.d.P.; Santos, K.d.F.; Bento, D.d.C.P.; da Silva Reis, A.A.; Santos, R.D. One-carbon metabolism pathway genes and their non-association with the development of amyotrophic lateral sclerosis. *J. Cell Biochem.* **2022**, *123*, 620–627. [CrossRef]
7. Sharma, M.; Tiwari, M.; Tiwari, R.K. Hyperhomocysteinemia: Impact on Neurodegenerative Diseases. *Basic. Clin. Pharmacol. Toxicol.* **2015**, *117*, 287–296. [CrossRef]
8. Moretti, R.; Caruso, P. The Controversial Role of Homocysteine in Neurology: From Labs to Clinical Practice. *Int. J. Mol. Sci.* **2019**, *20*, 231. [CrossRef]
9. Kim, Y. Folate and colorectal cancer: An evidence-based critical review. *Mol. Nutr. Food Res.* **2007**, *51*, 267–292. [CrossRef]
10. Coppedè, F.; Stoccoro, A.; Tannorella, P.; Gallo, R.; Nicolì, V.; Migliore, L. Association of Polymorphisms in Genes Involved in One-Carbon Metabolism with MTHFR Methylation Levels. *Int. J. Mol. Sci.* **2019**, *20*, 3754. [CrossRef]
11. Chen, J.; Bassot, A.; Giuliani, F.; Simmen, T. Amyotrophic Lateral Sclerosis (ALS): Stressed by Dysfunctional Mitochondria-Endoplasmic Reticulum Contacts (MERCs). *Cells* **2021**, *10*, 1789. [CrossRef]
12. Borgese, N.; Iacomino, N.; Colombo, S.F.; Navone, F. The Link between VAPB Loss of Function and Amyotrophic Lateral Sclerosis. *Cells* **2021**, *10*, 1865. [CrossRef]
13. Little, J.; Higgins, J.P.T.; Ioannidis, J.P.A.; Moher, D.; Gagnon, F.; Von Elm, E.; Khoury, M.J.; Cohen, B.; Davey-Smith, G.; Grimshaw, J.; et al. STrengthening the Reporting of Genetic Association Studies (STREGA)—An extension of the STROBE Statement. *PLoS Med.* **2009**, *6*, e1000022. [CrossRef]
14. National Center for Biotechnology Information. Available online: https://www.ncbi.nlm.nih.gov (accessed on 15 August 2023).
15. UniProt. Available online: https://www.uniprot.org/ (accessed on 6 August 2023).
16. Protein Data Bank (PDB). Available online: https://www.rcsb.org/ (accessed on 7 April 2023).
17. SNAP2. Available online: https://github.com/Rostlab/SNAP2 (accessed on 15 May 2023).
18. Hecht, M.; Bromberg, Y.; Rost, B. Better prediction of functional effects for sequence variants. *BMC Genom.* **2015**, *16*, S1. [CrossRef]
19. PolyPhen-2. Available online: http://genetics.bwh.harvard.edu/pph2/ (accessed on 7 May 2023).
20. Adzhubei, I.A.; Schmidt, S.; Peshkin, L.; Ramensky, V.E.; Gerasimova, A.; Bork, P.; Kondrashov, A.S.; Sunyaev, S.R. A method and server for predicting damaging missense mutations. *Nat. Methods* **2010**, *7*, 248–249. [CrossRef]
21. Mirdita, M.; Schütze, K.; Moriwaki, Y.; Heo, L.; Ovchinnikov, S.; Steinegger, M. ColabFold: Making protein folding accessible to all. *Nat. Methods* **2022**, *19*, 679–682. [CrossRef]
22. Marx, V. Method of the Year: Protein structure prediction. *Nat. Methods* **2022**, *19*, 5–10. [CrossRef]
23. Tunyasuvunakool, K.; Adler, J.; Wu, Z.; Green, T.; Zielinski, M.; Žídek, A.; Bridgland, A.; Cowie, A.; Meyer, C.; Laydon, A.; et al. Highly accurate protein structure prediction for the human proteome. *Nature* **2021**, *596*, 590–596. [CrossRef]
24. Yuan, S.; Chan, H.C.S.; Hu, Z. Using PyMOL as a platform for computational drug design. *Wiley Interdiscip. Rev. Comput. Mol. Sci.* **2017**, *7*, e1298. [CrossRef]
25. Nishimura, A.L. A novel locus for late onset amyotrophic lateral sclerosis/motor neurone disease variant at 20q13. *J. Med. Genet.* **2004**, *41*, 315–320. [CrossRef]
26. Kumar, C.V.; Kumar, K.M.; Swetha, R.; Ramaiah, S.; Anbarasu, A. Protein aggregation due to nsSNP resulting in P56S VAPB protein is associated with amyotrophic lateral sclerosis. *J. Theor. Biol.* **2014**, *354*, 72–80. [CrossRef] [PubMed]
27. Nunes Gonçalves, J.P.; Leoni, T.B.; Martins, M.P.; Peluzzo, T.M.; Dourado, M.E.T.; Saute, J.A.M.; Covaleski, A.P.; de Oliveira, A.S.; Claudino, R.; Marques, W., Jr.; et al. Genetic epidemiology of familial ALS in Brazil. *Neurobiol. Aging* **2021**, *102*, e1–e227. [CrossRef]
28. Liew, S.-C.; Gupta, E.D. Methylenetetrahydrofolate reductase (MTHFR) C677T polymorphism: Epidemiology, metabolism and the associated diseases. *Eur. J. Med. Genet.* **2015**, *58*, 1–10. [CrossRef]
29. He, R.; Yan, X.; Guo, J.; Xu, Q.; Tang, B.; Sun, Q. Recent Advances in Biomarkers for Parkinson's Disease. *Front. Aging Neurosci.* **2018**, *10*, 305. [CrossRef]
30. Zara-Lopes, T.; Gimenez-Martins, A.P.; Nascimento-Filho, C.H.; Castanhole-Nunes, M.M.; Galbiatti-Dias, A.L.; Padovani-Júnior, J.A.; Maniglia, J.V.; Francisco, J.L.; Pavarino, E.C.; Goloni-Bertollo, E.M. Role of MTHFR C677T and MTR A2756G polymorphisms in thyroid and breast cancer development. *Genet. Mol. Res.* **2016**, *15*, gmr.15028222. [CrossRef] [PubMed]
31. Abhinand, P.A.; Shaikh, F.; Bhakat, S.; Radadiya, A.; Bhaskar, L.V.; Shah, A.; Ragunath, P.K. Insights on the structural perturbations in human MTHFR Ala222Val mutant by protein modeling and molecular dynamics. *J. Biomol. Struct. Dyn.* **2016**, *34*, 892–905. [CrossRef]
32. Tanwar, H.; Sneha, P.; Thirumal Kumar, D.; Siva, R.; Walter, C.E.J.; George Priya Doss, C. A Computational Approach to Identify the Biophysical and Structural Aspects of Methylenetetrahydrofolate Reductase (MTHFR) Mutations (A222V, E429A, and R594Q) Leading to Schizophrenia. In *Advances in Protein Chemistry and Structural Biology*, 1st ed.; Donev, R., Ed.; Biomed Consult Ltd.: Swansea, UK, 2017; Volume 108, pp. 105–125. [CrossRef]
33. Desai, M.; Chauhan, J.B. Computational analysis for the determination of deleterious nsSNPs in human MTHFR gene. *Comput. Biol. Chem.* **2018**, *74*, 20–30. [CrossRef]

34. Shivkar, R.R.; Gawade, G.C.; Padwal, M.K.; Diwan, A.G.; Mahajan, S.A.; Kadam, C.Y. Association of MTHFR C677T (rs1801133) and A1298C (rs1801131) Polymorphisms with Serum Homocysteine, Folate and Vitamin B12 in Patients with Young Coronary Artery Disease. *Indian. J. Clin. Biochem.* **2022**, *37*, 224–231. [CrossRef]
35. Ebrahimi, A.; Colagar, A.H.; Karimian, M. Association of Human Methionine Synthase-A2756G Transition with Prostate Cancer: A Case-Control Study and in Silico Analysis. *Acta Med. Iran.* **2017**, *55*, 297–303.
36. Periñán, M.T.; Macías-García, D.; Jesús, S.; Martín-Rodríguez, J.F.; Muñoz-Delgado, L.; Jimenez-Jaraba, M.V.; Buiza-Rueda, D.; Bonilla-Toribio, M.; Adarmes-Gómez, A.D.; Gómez-Garre, P.; et al. Homocysteine levels, genetic background, and cognitive impairment in Parkinson's disease. *J. Neurol.* **2023**, *270*, 477–485. [CrossRef]
37. Fan, Y.; Wu, L.; Zhuang, W. Methylenetetrahydrofolate Reductase Gene rs1801133 and rs1801131 Polymorphisms and Essential Hypertension Risk: A Comprehensive Analysis. *Cardiovasc. Ther.* **2022**, *2022*, 2144443. [CrossRef] [PubMed]
38. Bailey, L.B. *Folate in Health and Disease*, 2nd ed.; CRC Press: Boca Raton, FL, USA, 2009; pp. 84–94.
39. Wan, L.; Li, Y.; Zhang, Z.; Sun, Z.; He, Y.; Li, R. Methylenetetrahydrofolate reductase and psychiatric diseases. *Transl. Psychiatry* **2018**, *8*, 242. [CrossRef] [PubMed]
40. Desai, M.; Chauhan, J.B. Predicting the functional and structural consequences of nsSNPs in human methionine synthase gene using computational tools. *Syst. Biol. Reprod. Med.* **2019**, *65*, 288–300. [CrossRef]
41. Naushad, S.M.; Devi, A.R.R.; Hussain, T.; Alrokayan, S.A.; Ramaiah, M.J.; Kutala, V.K. In silico analysis of the structural and functional implications of SLC19A1 R27H polymorphism. *J. Genet.* **2019**, *98*, 85. [CrossRef]
42. Skolnick, J.; Gao, M.; Zhou, H.; Singh, S. AlphaFold 2: Why It Works and Its Implications for Understanding the Relationships of Protein Sequence, Structure, and Function. *J. Chem. Inf. Model.* **2021**, *61*, 4827–4831. [CrossRef]
43. Guo, H.B.; Perminov, A.; Bekele, S.; Kedziora, G.; Farajollahi, S.; Varaljay, V.; Hinkle, K.; Molinero, V.; Meister, K.; Hung, C.; et al. AlphaFold2 models indicate that protein sequence determines both structure and dynamics. *Sci. Rep.* **2022**, *12*, 10696. [CrossRef]